Understanding Na Mobility in NASICON Materials: A Rietveld, 23Na and 31P MAS NMR, and Impedance Study

ARTICLE *in* CHEMISTRY OF MATERIALS · JANUARY 1998

Impact Factor: 8.35 · DOI: 10.1021/cm970648j

3 AUTHORS, INCLUDING:

Miguel A. G. Aranda
ALBA synchrotron Light Source - Barcelona, …
257 PUBLICATIONS **5,503** CITATIONS

SEE PROFILE

Sebastián Bruque
University of Malaga
123 PUBLICATIONS **2,603** CITATIONS

SEE PROFILE

Understanding Na Mobility in NASICON Materials: A Rietveld, ^{23}Na and ^{31}P MAS NMR, and Impedance Study

Enrique R. Losilla, Miguel A. G. Aranda,* and Sebastián Bruque

Departamento de Química Inorgánica, Cristalografía y Mineralogía, Universidad de Málaga, 29071 Málaga, Spain

Miguel A. París and Jesús Sanz

Instituto de Ciencia de Materiales, CSIC, Cantoblanco, 28049 Madrid, Spain

Anthony R. West

Department of Chemistry, University of Aberdeen, Meston Walk, Aberdeen AB24 3UE, U.K.

Received September 26, 1997. Revised Manuscript Received November 14, 1997

The structures and electrical properties of four NASICON compositions, $Na_{1.4}M_{1.6}In_{0.4}(PO_4)_3$ (M = Ti, Sn, Hf, Zr), have been determined and compared. Rietveld refinement of powder X-ray diffraction data confirmed the basic rhombohedral NASICON structure with random occupancy of the octahedral In/M sites, full occupancy of the Na(1) sites and partial occupancy of the Na(2) sites. For three compositions, M = Zr, Sn, and Hf, the ^{31}P MAS NMR peak intensities of the four detected signals, attributed to four different phosphorus environments $[P(OM)_{4-n}(OIn)_n$ $(n = 0-3)]$, were close to the ratios expected for a random distribution of In/M. For M = Ti, some departures from statistical occupancy were apparent. ^{23}Na MAS NMR data gave evidence for two Na^+ positions at room temperature for M = Ti, Sn, attributable to occupation of Na(1) and Na(2) sites. For M = Hf, Zr, only a single signal could be resolved at room temperature, which splits into two signals on cooling to − 50 °C, indicating high Na mobility at room temperature. Impedance data obtained on pressed sintered pellets over the range 25−300 °C showed that bulk ionic conductivities increased and activation energies decreased in the sequence Ti, Sn, Hf, Zr. The geometry of the M1M2 bottleneck has been determined from structural data, and a direct correlation found between activation energy for ion conduction and the bottleneck size.

Introduction

NASICON materials $Na_{1+x}Zr_2P_{3-x}Si_xO_{12}$ $(0 \le x \le 3)$ are well-known due to their high Na^+ mobility within a three-dimensional rhombohedral $R\bar{3}c$ network.[1,2] There are many papers devoted to structurally related compounds such as $Na_{1+x}M^{IV}_{2-x}M^{III}_x(PO_4)_3$, and some of these studies have tried to correlate crystal structure and ionic conductivity.[3,4] In the 3D skeleton, described by the formula $[M^{IV}_{2-x}M^{III}_x(PO_4)_3]^{(1+x)-}$, PO_4 tetrahedra are linked by their corners to MO_6 octahedra. The infinite ribbons resulting from this linkage are connected together, perpendicular to the *c* direction, by PO_4 tetrahedra to form the NASICON framework (Figure 1). The Na^+ ions can occupy two positions in the conduction channels: the M1 site (one per formula) is coordinated by a trigonal antiprism of oxygens, and the M2 site (three per formula) has a distorted 8-fold coordination. M1 and M2 sites are located inside and between the ribbons, respectively. The literature agrees

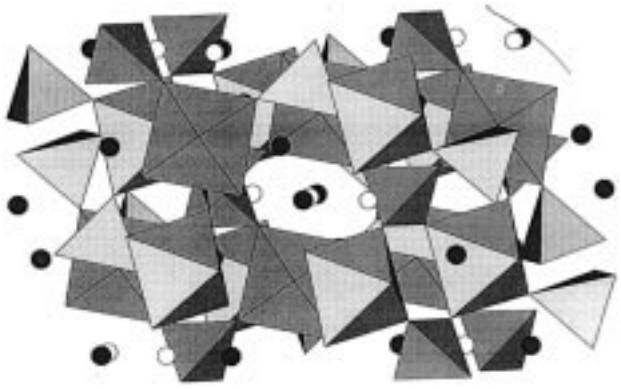

Figure 1. Polyhedral projection of the NASICON structure perpendicular to a set of M1···M2···M1···M2 channels. All possible M2 sites (black circles) are displayed, although only a fraction ≈15% are occupied by Na cations in $Na_{1.4}M_{1.6}In_{0.4}(PO_4)_3$ (M = Ti, Sn, Zr, Hf. The M1) site (white circles) are fully occupied by Na in these materials.

that there is a full occupancy of the M1 sites for $x = 0$ and that the M2 sites start to be filled for $x > 0$.

Most authors agree that structural features are the key to explaining the conduction mechanism, but the relevant structural parameters have not yet been identified. Some authors found correlations with ionic radii

(1) Hong, H. Y.-P. *Mat. Res. Bull.* **1976**, *11*, 173.
(2) Goodenough, J. B.; Hong, H. Y.-P; Kafalas, J. A.; *Mater. Res. Bull.* **1976**, *11*, 203.
(3) Tran-Qui, D.; Caponi, J. J.; Gondrand, M.; Saib, M.; Joubert, J. C.; Shannon, R. D. *Solid State Ionics*, **1981**, *3/4*, 219.
(4) Kholer, H.; Schulz, H. *Mater. Res. Bull.* **1986**, *21*, 23.

S0897-4756(97)00648-0 CCC: $15.00
Published on Web 01/10/1998

of the octahedrally coordinated cations, and others with unit-cell parameters, *a* and *c* or the cell volume.[5,6] This initial approach was followed by the scrutiny of factors such as the size of the bottleneck that connects M1 and M2 sites.[4,7,8] To establish this type of correlation, however, the full crystal structure determination by either single-crystal diffraction or by Rietveld analysis of powder diffraction data is necessary. Other factors that affect conductivity include the nature of the octahedral cations. For instance, NASICONS with main-group metals in the octahedral sites usually have lower conductivities than similar ones containing transition metals.[6,9]

The increase in the number of carriers (in this case expressed by $1 + x$) improves the conductivity up to a limiting value that depends on the material (for instance, σ_{max} occurs at $x = 2$ in NASICON silicophosphates). There is general agreement that it is necessary to have mobile cations partially distributed over several sites and that stoichiometric materials are comparatively much poorer ionic conductors. However, it is often difficult to compare reported data as it is common to find discrepancies in the conductivities for a given phase depending upon a number of factors: (1) preparation method, (2) thermal history,[10] (3) true bulk stoichiometry, (4) sintering processes,[11] and hence (5) possible influence of grain-boundary effects. Due to these factors, it appears that some degree of nonreproducibility is unavoidable and should be kept in mind when comparing results of different authors.

In the present work, we have attempted to understand the relation betwen Na mobility and structure in the series $Na_{1.4}M_{1.6}In_{0.4}(PO_4)_3$: M = Ti, Sn, Hf, Zr. The choice of materials with different metals M and this particular stoichiometry have been made so as to use a common synthetic method that results in the usual *R* $\bar{3}$*c* rhombohedral symmetry over a wide range of temperatures. The combined use of X-ray powder diffraction (Rietveld method), ^{31}P and ^{23}Na MAS NMR, and impedance spectroscopies has provided a better understanding of structural factors that control Na ion conduction, establishing conclusions that can be extended to other ion conduction systems.

Experimental Section

Synthesis. Stoichiometric amounts of Na_2CO_3, In_2O_3, $(NH_4)_2HPO_4$, and MO_2, synthesized as described below, were ground together and heated in a Pt crucible up to 1100 °C to give the following overall reaction:

$$0.7Na_2CO_3 + 1.6MO_2 + 0.2In_2O_3 + 3(NH_4)_2HPO_4 \xrightarrow{\Delta} Na_{1.4}M_{1.6}In_{0.4}(PO_4)_3 + 0.7CO_2 + 6NH_3 + 4.5H_2O$$

The tetravalent metal oxide starting materials were prepared as follows. MO_2 (M = Ti, Zr) were synthesized by slow hydrolysis (with 1:4 water/2-propanol ratio) of commercial alkoxides: 97% $Ti(OCH(CH_3)_2)_4$ and a solution of 70% $Zr(OCH_2CH_2CH_3)_4$ in 1-propanol. The resulting white suspensions were centrifuged, washed thoroughly with water, and heated at 200 °C for 2 h. SnO_2 was prepared from commercial $SnCl_4 \cdot 5H_2O$ by hydrolysis with NH_3(aq) to pH = 9. The white solid was centrifuged, washed with water to pH = 7, and heated at 200 °C for 2 h. The MO_2 (M = Ti, Sn, Zr) solids showed amorphous X-ray powder diffraction (XRD) profiles, and thermogravimetric analyses (TGA) did show small weight losses up to 700 °C which were taken into account for the NASICONs syntheses. HfO_2 (Aldrich, 99.8%) with microparticle size < 1 μm was dried at 200 °C and used without further treatment.

Table 1. Occupancy of Octahedral Site by In Determined by XRD and NMR (^{31}P MAS NMR Intensity Ratios of Adjacent Peaks Used To Calculate the M/In Ratio in Octahedral Sites)

sample	$4I_0/I_1$	$6I_1/4I_2$	$4I_2/6I_3$	$I_3/4I_4$	M^{4+}/In^{3+}	In (NMR)	In (XRD)
$Ti_{1.6}In_{0.4}$	2.5	3.7	5.2		3.21	0.47	0.39(1)
$Sn_{1.6}In_{0.4}$	3.6	4.3	2.8		3.75	0.42	0.45(5)
$Zr_{1.6}In_{0.4}$	3.3	3.9	3.9		3.61	0.43	0.43(3)
$Hf_{1.6}In_{0.4}$	4.8	4.2	3.6		4.50	0.36	0.42(4)

The starting mixtures were ground in an agate mortar with ethanol for 1 h, dried, heated at 0.5 °C min^{-1} to 400 °C, and left at that temperature for 1 day to release gases (NH_3, H_2O, and CO_2). To avoid/minimize the formation of byproducts, MP_2O_7 and unreacted MO_2, the samples were heated at 0.5 °C min^{-1} to 1000 °C with intermediate regrindings (for 30 min every 150 °C). Finally, the samples were left at 1000 °C for 2 days and 1100 °C for 3 days.

Thermal Characterization. TGA and differential thermal analysis (DTA) was carried out in air on a Rigaku Thermoflex TG 8110 apparatus from room temperature to 1100 °C at a heating rate of 10 °C/min with calcined Al_2O_3 as the reference.

X-ray Diffraction Characterization. The powder patterns were collected at room temperature in a Siemens D5000 diffractometer with ($\theta/2\theta$) Bragg−Brentano geometry. For phase purity assessment and indexing purposes, data were recorded between 13 and 50° 2θ. To refine the crystal structures by the Rietveld method,[12] data were collected between 13 and 125° 2θ with 0.03° step size and 16 s counting time.

MAS NMR Characterization. ^{31}P and ^{23}Na MAS NMR spectra were obtained between 25 and −50 °C using a B-VT 1000/SU07 unit adapted to a MSL 400 Bruker spectrometer. The frequencies used for ^{31}P and ^{23}Na spectra were 161.96 and 105.84 MHz. Samples were spun in the range 3−4 kHz, and spectra taken after $\pi/2$ pulse irradiation. A time interval between successive scans in the range 2−90 s was chosen, depending on the spin−lattice relaxation times of nuclei at the analyzed temperatures. The number of scans was in the range 10−30. The ^{23}Na and ^{31}P chemical shift values are given relative to 1 M NaCl and 85% H_3PO_4 aqueous solutions, respectively. Quantitative analyses of spectra were carried out with the WINFIT (Bruker) program. This program allows the position, line width, and intensity of the components of an experimental profile to be determined by using a standard nonlinear least-squares method.

Ionic Conductivity Characterization. Cylindrical pellets (≈10 mm diameter and ≈1 mm thickness) of the samples were obtained by applying uniaxial pressure of 200 MPa. The pellets were heated to achieve good sintering at 1150 °C (M = Ti) and 1300 °C (M = Sn, Hf, and Zr). The porosity estimated from the pellet mass and geometry was 17%, 21%, 29%, and 32% for M = Ti, Sn, Hf, and Zr, respectively. In−Ga alloy

(5) Delmas, C.; Olazcuaga, R.; Le Flem, G.; Hagenmuller, P.; Cherkaoui, F.; Brochu, R. *Mater. Res. Bull.* **1981**, *16*, 285.
(6) Winand, J. M.; Rulmond, A.; Tarte, P. *J. Mater. Sci.* **1990**, *25*, 4008.
(7) Kholer, H.; Schulz, H. *Mater. Res. Bull.* **1985**, *20*, 1461.
(8) Kholer, H.; Schulz, H. *Solid State Ionics* **1983**, *9/10*, 795.
(9) Saito, Y.; Ado, K.; Asai, T.; Kageyama, H.; Nakamura, O. *Solid State Ionics* **1992**, *58*, 327.
(10) Gusakovskaya, I. G.; Pirumova, S. I. *Russ. J. Inorg. Chem. (Engl. Transl.)* **1994**, *39*, 1221.
(11) (a) Aono, H.; Sugimoto, E.; Sadaoka, Y.; Imanaka, N.; Adachi, G. *J. Electrochem. Soc.* **1990**, *137*, 1023. (b) Aono, H.; Sugimoto, E.; Sadaoka, Y.; Imanaka, N.; Adachi, G. *Solid State Ionics* **1993**, *62*, 309.
(12) Rietveld, H. M. *J. Appl. Crystallogr.* **1969**, *2*, 65.

Table 2. Crystallograpic and Conductivity Parameters for $Na_{1+x}M_{2-x}In_x(PO_4)_3$

M	x	R_{WP}/%	R_F/%	X^2	a/Å	c/Å	V/Å^3	σ_{400K}/S cm^{-1}	σ_{600K}/S cm^{-1}	$E_a(\sigma)$/eV	E_a(fmax)/eV
Ti	0				8.485	21.801	1359.2	3.7×10^{-7}	2.3×10^{-5}	0.47[a]	
	0.4	13.0	6.0	2.5	8.5753(1)	21.9048(4)	1394.96(3)	2.8×10^{-6}	4.86×10^{-4}	0.535	0.60
Sn	0				8.513	22.511	1412.9	4.5×10^{-9}	6.4×10^{-7}	0.58[a]	
	0.4	14.7	2.9	4.0	8.6662(2)	22.3485(5)	1453.57(6)	3.9×10^{-6}	6.13×10^{-4}	0.530	0.58
Hf	0				8.763	22.666	1507.5	5.1×10^{-7}	4.9×10^{-5}	0.51[a]	
	0.4	12.6	4.1	4.8	8.8182(1)	22.6157(2)	1522.99(2)	7.7×10^{-6}	3.59×10^{-4}	0.405	0.50
Zr	0				8.804	22.759	1527.7	1.2×10^{-6}	7.5×10^{-5}	0.47[a]	
	0.4	11.7	3.2	3.5	8.8363(1)	22.7061(5)	1535.38(5)	6.8×10^{-5}	2.41×10^{-3}	0.400	0.40

[a] Data taken from ref 17.

(approximately 1:1) was applied onto the flat pellet faces to form electrodes. The ionic conductivity data were collected using a Hewlett-Packard 4192A impedance analyzer over the frequency range 50 Hz to 13 MHz. The samples were studied from room temperature to 300 °C, at 30 °C intervals.

Results

The initial XRD data indicated that the four phases were highly crystalline with structures belonging to the rhombohedral $R\bar{3}c$ NASICON-type. $Na_{1.4}M_{1.6}In_{0.4}(PO_4)_3$ (M = Ti, Hf, Zr) were single phase by XRD. A small amount of cassiterite (SnO_2 oxide) was detected in the $Na_{1.4}Sn_{1.6}In_{0.4}(PO_4)_3$ sample. Thermal analysis showed the absence of phase transitions between room temperature and 1100 °C.

Rietveld Study. The crystal structures of all four phases were refined from XRD data by the Rietveld method using the $R\bar{3}c$ structure of $NaZr_2(PO_4)_3$ as starting model.[1] The nominal M/In composition was assumed to be randomly distributed at the octahedral site. Full occupancy of the Na(1) site at (000) (6b Wyckoff notation) and the excess sodium located in the Na(2) site at (0.65 0 $^1/_4$) (18e) was initially postulated. The common overall parameters, histogram scale factor, background coefficients, unit-cell parameters, zero-shift error, and pseudo-Voigt coefficients[13] corrected for asymmetry[14] were refined first. Then, the positional parameters were optimized. After convergence, the fraction of In at the metal(IV) site was allowed to vary but constrained to full occupancy of the site. The occupation factors of Na(2) site were refined in such a way that electroneutrality of the refined chemical formula was maintained. Finally, the temperature factors of different sites were refined freely. Refinements of the Na(1) site occupancy indicated full occupancy for M = Sn, Hf, and Zr but slightly lower occupancy for M = Ti.

As Sn and In are adjacent elements in the periodic table, these cannot be distinguished by XRD. Hence, the occupancy of Sn was set to 1.00, and the amount of Na at the M(2) site was refined freely, which indirectly indicates the degree of substitution of Sn by In. The presence of cassiterite was taken into account in the Rietveld refinement. The relative amounts of the two phases was 97.9(1) mol % $Na_{1.45}Sn_{1.55}In_{0.45}(PO_4)_3$ (99.43(3) mass %) and 2.1 mol % SnO_2 (0.57 mass %).

The refined metal ratios (summarized in Table 1) agree very well with the nominal starting compositions which indicates that the mixtures reacted thoroughly to produce the desired NASICON materials. Only for M = Sn was a second minor phase, SnO_2, observed. The refined Na composition indicates a Sn/In ratio of 1.55/0.45(5). This is the highest In content in all NASICON phases studied and higher than the nominal starting composition 1.60/0.40. In the other three samples, the refined metal ratios are closer to the nominal compositions and secondary phases were not observed by XRD.

A summary of the refinement results that includes the agreement factors and the unit cell parameters is given in Table 2. The refined atomic parameters are given in Tables 3−6 and bond distances in Table 7. As an example of the Rietveld refinement quality, the fit to the X-ray pattern for $Na_{1.4}Zr_{1.6}In_{0.4}(PO_4)_3$ is shown in Figure 2.

Table 3. Structural Parameters for $Na_{1.39}Ti_{1.61}In_{0.39}(PO_4)_3$

atom	site sym	x	y	z	frac	U_{iso}/Å^2
Na(1)	6b	0	0	0	0.949(10)	0.036(3)
Na(2)	18e	0.649(4)	0	0.25	0.146(3)	0.049(10)
Ti/In	12c	0.00	0.00	0.14611(7)	0.806(5)/0.194	0.0060(6)
P	18e	0.2893(3)	0.00	0.25	1.00	0.0088(8)
O(1)	36f	0.1755(5)	−0.0303(6)	0.1935(2)	1.00	0.018(1)
O(2)	36f	0.1917(5)	0.1625(5)	0.0875(2)	1.00	0.012(1)

Table 4. Structural Parameters for $Na_{1.45}Sn_{1.55}In_{0.45}(PO_4)_3$

atom	site sym	x	y	z	frac	U_{iso}/Å^2
Na(1)	6b	0	0	0	1.00	0.044(3)
Na(2)	18e	0.619(8)	0	0.25	0.15(2)	0.11(4)
Sn/In	12c	0.00	0.00	0.14698(6)	1.00	0.0044(4)
P	18e	0.2953(5)	0.00	0.25	1.00	0.004(1)
O(1)	36f	0.1851(10)	−0.0314(11)	0.1943(4)	1.00	0.024(3)
O(2)	36f	0.1903(7)	0.1675(9)	0.0862(3)	1.00	0.011(2)

Table 5. Structural Parameters for $Na_{1.42}Hf_{1.58}In_{0.42}(PO_4)_3$

atom	site sym	x	y	z	frac	U_{iso}/Å^2
Na(1)	6b	0	0	0	1.00	0.055(4)
Na(2)	18e	0.593(8)	0	0.25	0.142(16)	0.09(4)
Hf/In	12c	0.00	0.00	0.14631(4)	0.79(2)/0.21	−0.0015(3)
P	18e	0.2954(5)	0.00	0.25	1.00	0.001(1)
O(1)	36f	0.1916(10)	−0.0144(11)	0.1960(3)	1.00	0.011(3)
O(2)	36f	0.1887(8)	0.1657(9)	0.0835(3)	1.00	0.006(2)

Table 6. Structural Parameters for $Na_{1.43}Zr_{1.57}In_{0.43}(PO_4)_3$

atom	site sym	x	y	z	frac	U_{iso}/Å^2
Na(1)	6b	0	0	0	1.00	0.050(3)
Na(2)	18e	0.618(6)	0	0.25	0.144(9)	0.10(3)
Zr/In	12c	0.00	0.00	0.14661(5)	0.783(14)/0.217	0.0030(4)
P	18e	0.2950(4)	0.00	0.25	1.00	0.006(1)
O(1)	36f	0.1884(7)	−0.0231(8)	0.1961(3)	1.00	0.013(2)
O(2)	36f	0.1917(6)	0.1692(6)	0.0855(2)	1.00	0.004(2)

(13) Thompson, P.; Cox, D. E.; Hasting, J. B. *J. Appl. Crystallogr.* **1987**, *20*, 79.
(14) Finger, L. W.; Cox, D. E.; Jephcoat, A. P. *J. Appl. Crystallogr.* **1994**, *27*, 892.

Table 7. Bond Distances (Å) for $Na_{1.4}M_{1.6}In_{0.4}(PO_4)_3$ (M = Ti, Sn, Hf, Zr)

	Ti	Sn	Hf	Zr
M−O(1) × 3	1.950(4)	2.049(7)	2.086(8)	2.102(6)
M−O(2) × 3	2.001(4)	2.068(6)	2.118(7)	2.121(5)
P−O(1) × 2	1.516(4)	1.509(8)	1.492(8)	1.494(6)
P−O(2) × 2	1.535(4)	1.509(6)	1.548(7)	1.525(5)
Na(1)−O(2) × 6	2.455(4)	2.479(6)	2.458(7)	2.519(5)
Na(2)−O(1) × 2	2.69(2)	2.91(5)	3.00(7)	3.01(4)
Na(2)−O(1) × 2	2.67(1)	2.66(1)	2.73(1)	2.74(1)
Na(2)−O(2) × 2	2.56(3)	2.32(5)	2.17(5)	2.35(4)
Na(2)−O(2) × 2	2.27(1)	2.39(1)	2.48(2)	2.44(1)

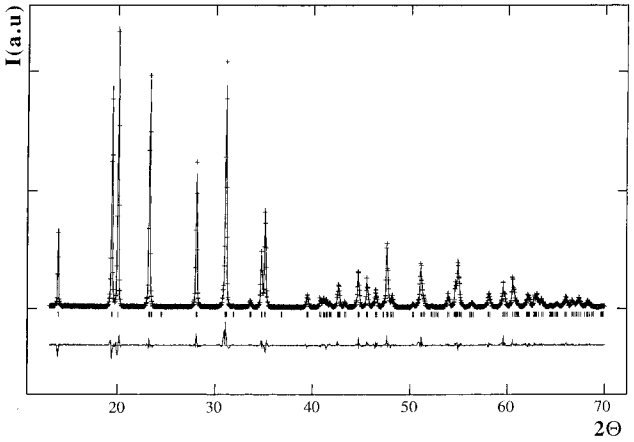

Figure 2. Observed, calculated and difference X-ray diffraction plots for $Na_{1.43}Zr_{1.57}In_{0.43}(PO_4)_3$. Reflection positions are marked.

^{31}P MAS NMR Study. ^{31}P MAS NMR spectra of the samples (Figure 3), taken at room temperature, are formed by four components with their corresponding spinning sidebands (not shown in Figure 3). In all cases, intensities of different components decrease when going toward more positive chemical shifts. In the Hf sample, the components exhibit similar line widths and their separation is lower than in the other samples. In these samples, the most intense component is considerably narrower than the others lines.

In the NASICON structure each tetrahedron shares oxygens with four octahedra: two in the same $M_2(PO_4)_3$ unit and two with other adjacent units. On the basis of a random distribution of tri and tetravalent cations, five possible environments for P atoms can be imagined in $Na_{1+x}M_{2-x}In_x(PO_4)_3$ phases: $P(OM)_4$, $P(OM)_3(OIn)_1$, $P(OM)_2(OIn)_2$, $P(OM)(OIn)_3$, $P(OIn)_4$. From statistical considerations, the four components detected must correspond to the first four of these environments.

The variations observed in the position of the $P(OM)_4$ component in the four samples is associated with differences in the polarizing strength of tetravalent cations (Table 8). In general, cations with smaller radii pull the electron density away from oxygen atoms more effectively, leaving the phosphorus atoms more positively charged. This produces a higher shielding effect on the ^{31}P NMR resonance, which explains the more negative σ_{iso} values observed. On the basis of the regular separation between components, the position of the nondetected component, associated with the $P(OIn)_4$ environment, can be extrapolated to occur between −6 and −9 ppm in all analyzed samples. This value confirms again the lower shielding effect of trivalent cations. A similar effect was reported in tectosilicates where tetravalent Si is substituted by trivalent Al.

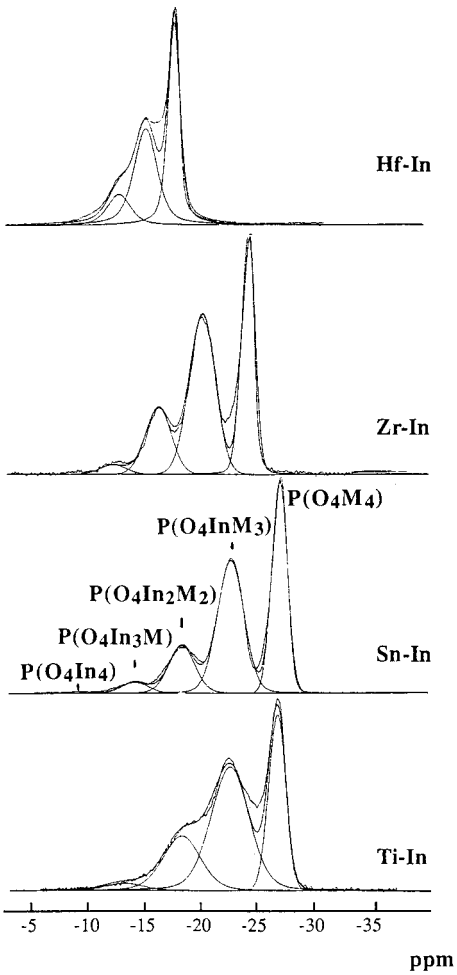

Figure 3. ^{31}P MAS NMR spectra for $Na_{1.4}M_{1.6}In_{0.4}(PO_4)_3$ (M = Ti, Sn, Zr, Hf).

Table 8. Chemical Shift Values of MAS NMR Components of $NaM_{2-x}In_x(PO_4)_3$ Samples[a]

sample	M_4	M_3In	M_2In_2	MIn_3	In_4
$Ti_{1.6}In_{0.4}$	−26.7	−22.5	−18.0	−12.7	(−8.5)
$Sn_{1.6}In_{0.4}$	−27.0	−22.6	−18.1	−13.8	(−9.3)
$Zr_{1.6}In_{0.4}$	−24.0	−19.7	−15.6	−11.5	(−7.0)
$Hf_{1.6}In_{0.4}$	−17.0	−13.9	−11.5	−9.0	(−6.5)

[a] The value for the In_4 environment is calculated by linear extrapolation, assuming a constant peak separation, from positions of the other components.

From the integrated intensities of the four observed ^{31}P NMR components, the chemical composition of samples can be estimated. In particular, M^{4+}/In^{3+} ratios (Table 1) can be calculated from the expression:

$$M^{4+}/In^{3+} = \frac{4I_0 + 3I_1 + 2I_2 + I_3}{1I_1 + 2I_2 + 3I_3 + 4I_4}$$

where I_i intensities, with $i = 0, 1, 2, 3$, and 4, correspond to components with increasing number of In atoms. From the M^{4+}/In^{3+} ratios, the M^{4+} $(2 - x)$ and In^{3+} (x) contents of the octahedral sites can be deduced using the expression

$$M^{4+}/In^{3+} = (2 - x)/x$$

The deduced occupancies (Table 1) are very close to the nominal values used in sample preparation and to those deduced from the Rietveld analyses.

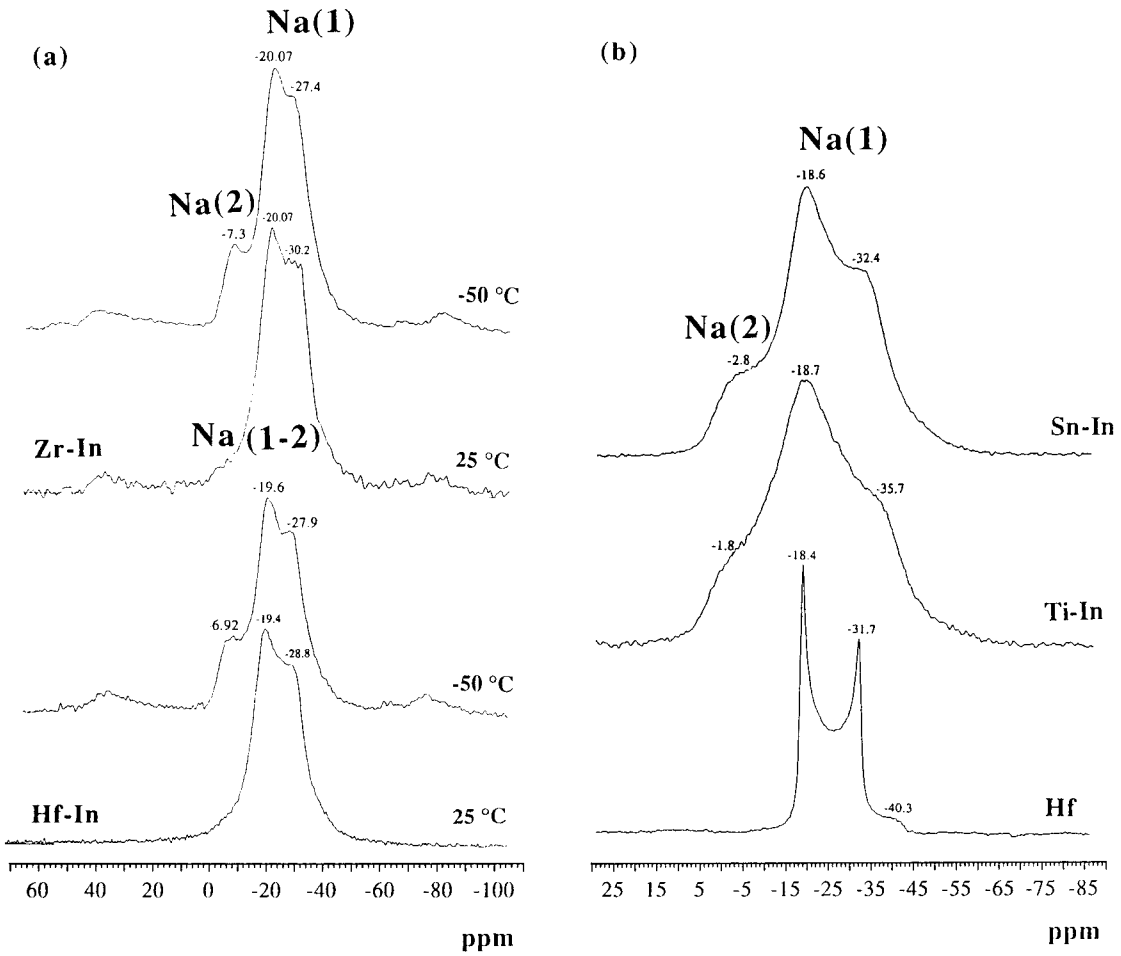

Figure 4. ^{23}Na MAS NMR spectra for (a) $Na_{1.4}M_{1.6}In_{0.4}(PO_4)_3$ (M = Hf, Zr) at room temperature and −50 °C; (b) $NaHf_2(PO_4)_3$ and $Na_{1.4}M_{1.6}In_{0.4}(PO_4)_3$ (M = Ti, Sn) at room temperature.

A random distribution of M^{4+} and In^{3+} cations in the octahedral site would give intensities of ^{31}P NMR components proportional to $(2 - x)^4$, $4(2 - x)^3x$, $6(2 - x)^2x^2$, $4(2 - x)x^3$, and x^4, respectively. From integrated intensities of adjacent components corrected for statistical multiplicity, the $(2 - x)/x$ ratio were again calculated (Table 1). These ratios ($4I_0/I_1$, $6I_1/4I_2$, $4I_2/6I_3$) are very similar for M = Zr, indicating a random distribution of the two metals at the octahedral site. For M = Ti, the bands associated with groups of higher In content, especially $P(OTi)_3(OIn)_1$ and $P(OTi)_2(OIn)_2$, are larger than expected from a statistical distribution which indicates that the cations are not homogeneously distributed and some departure from statistical distribution is present. The situation for M = Sn, Hf is intermediate. It shoud be pointed out that the values given in the $4I_2/6I_3$ column are affected by larger errors due to the low intensities of the I_3 bands.

^{23}Na MAS NMR Study. ^{23}Na MAS NMR spectra were recorded for $Na_{1.4}M_{1.6}In_{0.4}(PO_4)_3$ (M = Hf, Zr) at room temperature and −50 °C (Figure 4a), and for $NaHf_2(PO_4)_3$ and $Na_{1.4}M_{1.6}In_{0.4}(PO_4)_3$ (M = Ti, Sn) at room temperature (Figure 4b). In this figure, the spectrum for $NaHf_2(PO_4)_3$, included as reference, displays two lines at −18.3 and −31.7 ppm with a small shoulder at −40.3 ppm. The observed pattern is produced by the second-order quadrupole interaction of Na nuclei at the Na(1) site with the electric field gradient. The NMR profile of the transition $-^1/_2$ to $^1/_2$ was fitted by a unique signal with an isotropic chemical shift of −14.2 ppm and quadrupole constants $C_Q = 2.27$ MHz and $\eta = 0$. The location of Na(1) on 3-fold axes accounts for the observed η value ($\eta = 0$) in $NaHf_2(PO_4)_3$, in agreement with the observation reported for isostructural $NaZr_2(PO_4)_3$.[15]

For M = Ti and Sn, three broad components are detected at ≈−3, −19, and −32/−36 ppm (Figure 4b). For M = Zr and Hf at room temperature, two main components are detected at −19 and −29 ppm (Figure 4a). On cooling these samples below −40 °C, the ^{23}Na spectra reveal the presence of a new component at −7 ppm (Figure 4a).

On the basis of the Rietveld analyses of $NaM_{2-x}In_x(PO_4)_3$ samples, one Na occupies M1 sites and the rest are distributed over the three symmetry-equivalent M2 sites. Hence, ^{23}Na spectra should give two signals, the main one with characteristics similar to those detected in $NaHf_2(PO_4)_3$. In all cases, MAS NMR spectra are formed by two main components with positions (−19 and −29/−32 ppm) near those detected in $NaHf_2(PO_4)_3$. However, the components are very broad indicating the existence of different environments for Na atoms.

In the case of Ti and Sn members, a third band is detected around −3 ppm in the ^{23}Na spectra. These

(15) Jäger, C.; Barth, S.; Feltz, A. *Chem. Phys. Lett.* **1989**, *154*, 45.

spectra have been analyzed by supposing the existence of two components: one is associated with Na cations located at M1 sites, with similar characteristics to Zr and Hf samples, and the other with Na cations at M2 sites. From the difference between the experimental envelope and the profile calculated for M1 sites, the quadrupole constants associated with the second environment was derived. The quadrupolar constants associated with the two Na sites of the Sn sample are $C_Q \approx 2.24$ MHz and $\eta = 0$ for M1 sites and $C_Q \approx 2.40$ MHz and $\eta = 0.7$ for M2 sites. The relative intensities of the two components agree reasonably well with those predicted on the basis of a preferential occupation of M1 sites (M2:M1 = 0.4:1). Asymmetry η values deduced for the two sites are very different, confirming that the point symmetry of the two sites is different. Chemical shifts of the two components, corrected for second-order quadrupolar effects, are −12 and 4 ppm, for Na at M1 and M2, respectively.

^{23}Na NMR spectra for Zr and Hf samples, recorded at room temperature, show the absence of the signal associated with M2 sites. This can be explained by assuming the existence of a significant mobility that enables Na cations to exchange between the M1 and M2 sites in the NMR measuring time scale. This phenomenon would produce a single averaged line displaying intermediate chemical shift and quadrupole constants. As the Na cations are preferentially located at M1 sites, the time spent by a Na atom at M1 sites should be higher than that spent at M2 sites and the resulting quadrupole constants would be similar to those of M1 sites. The somewhat greater line widths measured for Na components in these samples suggests that some heterogeneity in the Na environment exists, probably due to mobility-related effects. When Na mobility is eliminated, by decreasing the temperature, the two environments for Na cations are resolved by ^{23}Na NMR spectroscopy (Figure 4a), with intensities that are near those of other samples and similar to those expected from Rietveld analyses.

Impedance Study. Impedance data in the form of a complex plane plot are shown for one sample, M = Ti, at two temperatures in Figure 5. These data are typical of all compositions. The data show a single, rather broad arc at high frequencies/low temperatures (a). With increasing temperature, lower frequency effects are seen, in the form of an inclined spike (b). This has an associated capacitance, given from the ideal relation $Z'' = (\omega C)^{-1}$, of about 0.6 μF. From these data, it may be concluded that the samples are ionic conductors and that the overall pellet resistance can be determined from the intercept of the low-frequency spike or the low-frequency end of the broadened semicircular arc, on the real, Z' axis.

To investigate the electrical microstructure of the pellets and in particular determine whether the overall pellet resistances represented the bulk resistance of the grains or were influenced by grain boundary effects, the experimental data were replotted as the imaginary parts of the impedance, Z″ and electric modulus, M″ against log frequency, as shown in Figure 6 for the four samples. The data for M = Zr showed single peaks in both the M″ and Z'' spectra, separated in frequency by about half a decade. The peaks are somewhat broader

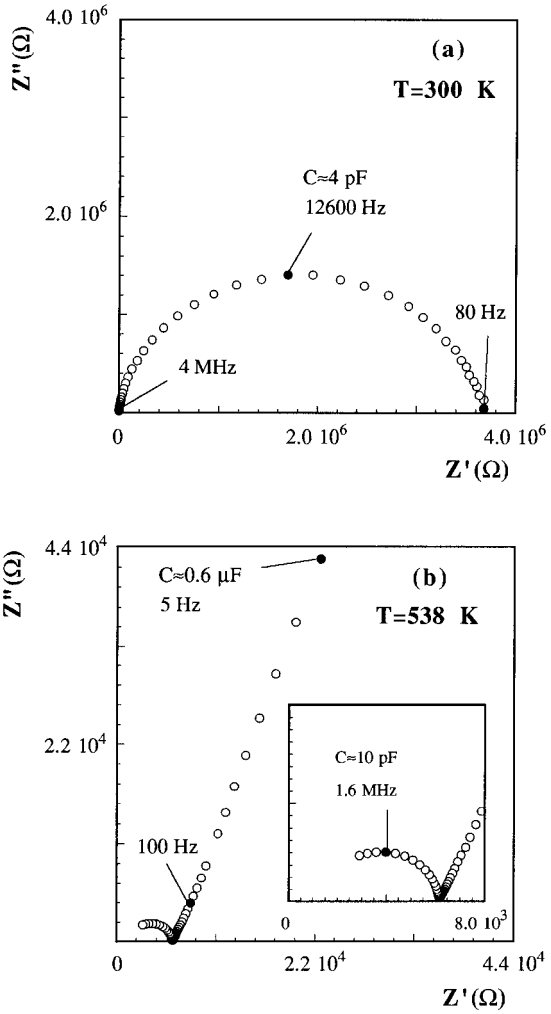

Figure 5. Impedance complex plane plot for $Na_{1.39}Ti_{1.61}In_{0.39}(PO_4)_3$ at (a) 300 K and (b) 538 K.

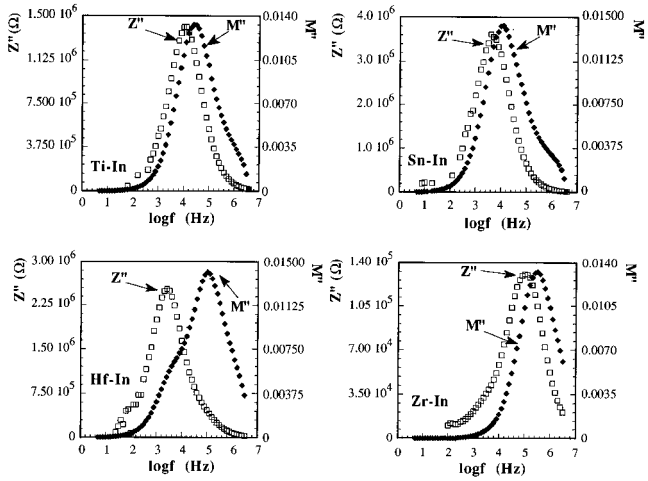

Figure 6. Impedance and modulus spectroscopic plots for $Na_{1.4}M_{1.6}In_{0.4}(PO_4)_3$ (M = Ti, Sn, Hf, Zr).

than an ideal Debye peak, with a peak width at half-height of ≈1.8 decades, compared to 1.14 decades for a Debye peak.

The height of the M'' peak, given by the relation $M''(\max) = Co/2C = 1/2\epsilon'$ for an ideal Debye peak, has a value of 0.0133, corresponding to a value of ϵ' of ≈38. This value is overestimated since the value of $M''(\max)$ is reduced as a consequence of (a) the peak broadening

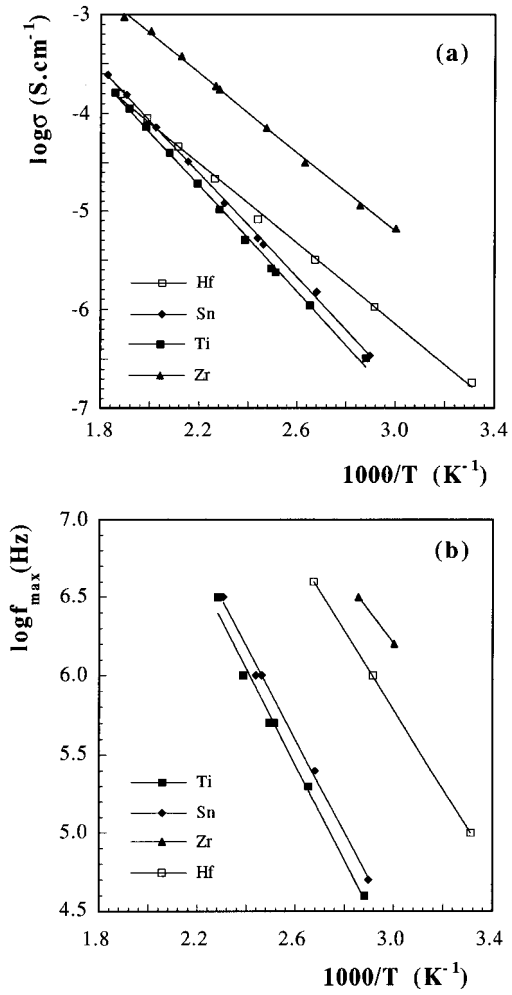

Figure 7. Arrhenius representations for $Na_{1.4}M_{1.6}In_{0.4}(PO_4)_3$ (M = Ti, Sn, Hf, Zr) of (a) log σ versus 1000/T and (b) log f(max) versus 1000/T.

and (b) the presence of stray capacitances associated with the experimental measuring arrangement. Since high-frequency bulk permittivities for ionic conductors have values typically of 10−20, it is clear that the M'' peak shown in Figure 6 represents the bulk response of the sample. Further, since the Z'', M'' peaks are almost coincident and there is no evidence of any additional peaks at lower frequencies in the Z'' spectrum, the Z'' peak and the corresponding Z^* complex plane plot also represent the bulk response of the sample. Impedance and modulus spectroscopy data for samples M = Ti, Sn (Figure 6) are quite similar to the Zr data and therefore, the conductivities extracted from the impedance complex plane plots also represent bulk conductivities.

The M''/Z'' spectroscopic plots for the M = Hf sample (Figure 6) are significantly different from those of the other compositions and show some variation with processing heat treatments. The M'' and Z'' maxima are separated by about 1.5 decades; the M'' plots show evidence of a shoulder peak at lower frequency at approximately the same position as the Z'' peak maximum. It is clear, therefore, that these samples contain two components; one dominates the M'' spectrum at high frequencies and, from the value of M''(max), this represents the bulk of the sample. The other dominates the Z'' spectrum at lower frequencies and therefore

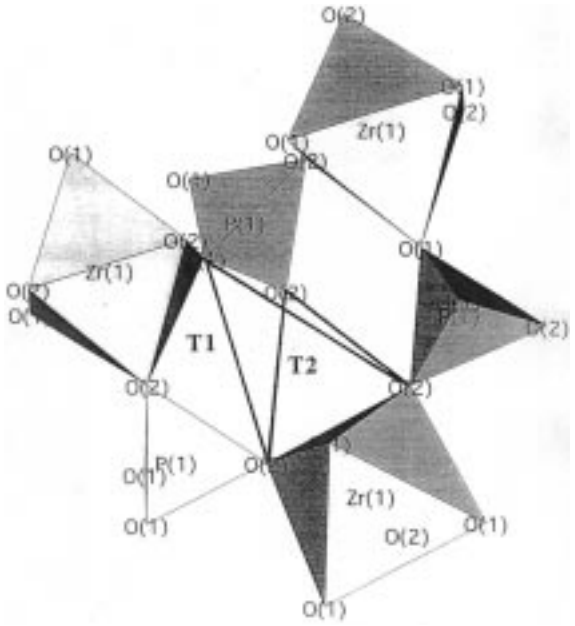

Figure 8. Polyhedral view of the M1M2 bottleneck formed by three ZrO_6 octahedral edges and three PO_4 tetrahedral edges. The triangles T1 and T2 are outlined. The Na(1) and Na(2) cations are located above and below the bottleneck.

forms the main component of the resistance of the pellet. It is attributed to a thick grain boundary effect, probably associated with the poor sintering of the ceramic.

The main conclusion for these Hf-containing samples, then, is that the Z'' spectra and hence the Z^* complex plane plots are dominated by the grain boundary component. Consequently, the Arrhenius conductivity plots for the four compositions (Figure 7a) correspond to the bulk data for M = Ti, Sn, and Zr but to grain-boundary-dominated data for M = Hf; this accounts for the apparently anomalous response of the M = Hf sample.

A better comparison of the intrinsic bulk conducting properties of the four compositions is obtained from Arrhenius plots of the frequency of the modulus peak maxima, M''(max) (Figure 7b). The M''(max) occurs, ideally, when $\omega RC = (2\pi f)RC = 1$; assuming that C is independent of temperature, then $f(\text{max}) \propto R^{-1}$ and hence the temperature dependence of f(max) reflects the temperature dependence of R. The data in Figure 7b show that f(max) increases with increasing temperature. For a given temperature, f(max) increases (and hence R decreases) in the sequence Ti $\lesssim$ Sn $\ll$ Hf $\lesssim$ Zr. The activation energies, given by the slopes of the Arrhenius plots (Table 2) also decrease in the same sequence.

Discussion

The unit cell a and c parameters of $Na_{1.4}M_{1.6}In_{0.4}(PO_4)_3$: M = Ti, Sn, Hf, Zr (Table 2) increase in the sequence Ti < Sn < Hf < Zr, consistent with the variation in the ionic radii of M.[16] When the unit-cell parameters of the parent phases, $NaM_2(PO_4)_3$, and their derivatives $Na_{1.4}M_{1.6}In_{0.4}(PO_4)_3$, are compared, an increase of a, a decrease of c, and an overall increase in

(16) Shannon, R. D. *Acta Crystallogr.* **1976**, *A32*, 751.
(17) Winand, J. M.; Rulmond, A. Tarte, P. *J. Solid State Chem.* **1991**, *93*, 341.

Table 9. Dimensions of M1M2 Triangular Bottleneck for $Na_{1.4}M_{1.6}In_{0.4}(PO_4)_3$ (M = Ti, Sn, Hf, Zr)

sample	O(2)···O(2)/ Å "common"	O(2)···O(2)′ × 2/ Å T2	area/ Å² T2	O(1)···O(2)′/ Å T1	O(2)···O(1)// Å T1	area/ Å² T1
$Ti_{1.6}In_{0.4}$	2.657	4.129	5.193	3.693	4.165	4.834
$Sn_{1.6}In_{0.4}$	2.702	4.157	5.311	3.674	4.189	4.897
$Hf_{1.6}In_{0.4}$	2.724	4.091	5.254	3.812	4.278	5.111
$Zr_{1.6}In_{0.4}$	2.778	4.201	5.507	3.798	4.305	5.198

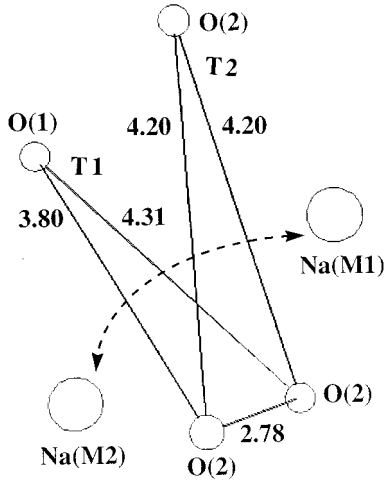

Figure 9. ORTEP view of the M1M2 bottleneck formed by the triangles T1 and T2 showing the pathway to jump from the M1 to the M2 site. The distances (Å) correspond to those in $Na_{1.43}Zr_{1.57}In_{0.43}(PO_4)_3$.

cell volume for each pair of phases is observed. The increase in volume is 2.6% for Ti, 2.9% for Sn, 1.0% for Hf, and 0.5% for Zr. Thus, the substitution of M(IV) by In(III) with the subsequent insertion of extra Na^+ ions expands the framework anisotropically and especially in the phases with less free volume, i.e., M = Ti and Sn. Earlier reports on the substitution of Zr(IV) by In(III) showed similar expansions in the *ab* plane and contractions in the *c* direction.[5,6]

The above comments relate to macroscopic or overall unit-cell data. However, the main objective of this work is to relate the structural characteristics, deduced from the XRD data, to the microscopic site and mobility information obtained from MAS NMR and to the ionic conductivity obtained from the impedance analysis. These materials have the same framework, symmetry, and overall cation ratios but significantly different local structures, affecting bottleneck sizes in the mobile ion conduction pathways.

A nonstandard view of the NASICON structure was presented in Figure 1. Long-range conduction of the Na ions in the NASICON structure involves hopping between Na(1) and Na(2) sites. These sites are joined by a bottleneck generally termed the M1M2 bottleneck. Symmetry-related infinite channels running in different directions are interconnected at the M1 site. A polyhedral view of the M1M2 bottleneck is given in Figure 8. The pseudo-hexagonal bottleneck is formed by three MO_6 octahedral edges and three PO_4 tetrahedral edges as previously pointed out by Hong.[1] Some authors have suggested that the important structural parameter to characterize the bottleneck is the size and shape of the (T2) triangle defined by three O(2) atoms shown in Figure 8. However, Kohler and Schulz[4,7,8] have suggested from the study of the probability density function (PDF) that the real M1M2 bottleneck is situated away

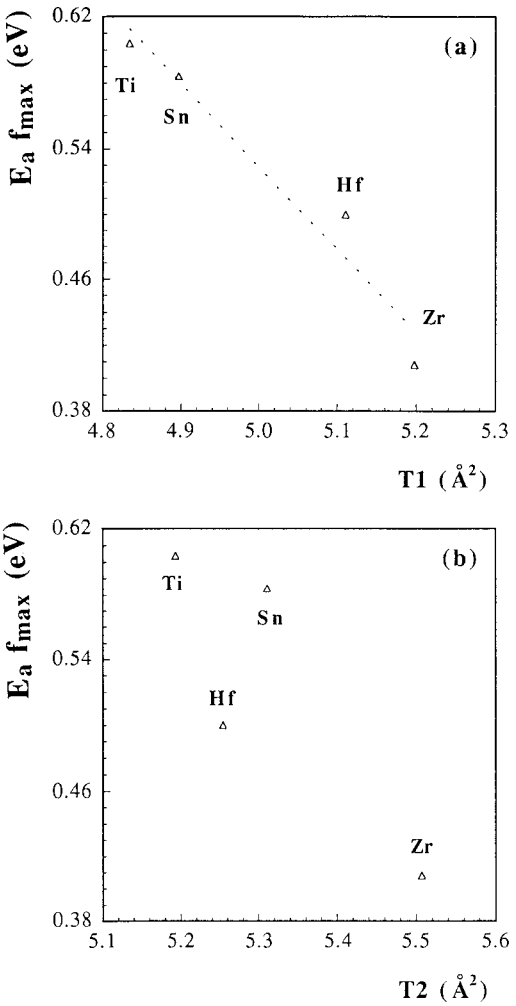

Figure 10. Variation of activation energy, E_a, with (a) area of triangle T1 and (b) area of triangle T2.

from the T2 triangle. These authors identified a second triangle T1 defined by one O(1) and two O(2) and suggested that the bottleneck of the M1M2 pathway is located between the T1 and T2 triangles. T1 and T2 are indicated by thick lines in Figure 8 and an ORTEP view of the pathway for a Na^+ ion to jump from the M1 site to the M2 site is shown in Figure 9. As the full structures are known, all distances between atoms can be calculated. The edges of the triangles T1 and T2 and their respective areas are given in Table 9. The areas for the T1 triangles are clearly smaller than those for the T2 triangles. Hence, it seems reasonable to suggest that it should be more difficult for Na^+ ions to pass between the oxygen atoms that define T1 than to pass between those that define T2.

We have sought correlations between these structural parameters determined from the XRD study and the mobility/conductivity data. In Figure 10, the areas of the T1 and T2 triangles are plotted against the activation energies for conduction from the f_{max} representa-

tion. Although there is no obvious correlation between T2 areas and E_a, there is a clear correlation between the T1 areas and E_a. In particular, as T1 areas become smaller, activation energies increase and the hopping process is disfavored; this is consistent with the much lower Na mobility, deduced from the ^{23}Na NMR study.

The changes observed in ^{23}Na MAS NMR spectra of the Hf and Zr materials on cooling have been assigned to a decrease of Na mobility. The averaging of the two signals due to Na(1) and Na(2) sites, induced by Na motion, is eliminated by cooling the sample. Conversely, increasing the temperature should result in loss of the Na(2) NMR signal in the spectra for Ti and Sn, as a consequence of the rapid exchange of Na between M1 and M2 sites. Further variable-temperature XRD and MAS NMR studies and isothermal impedance investigation are in progress to characterize this two-state transition.

Conclusions

(1) The multitechnique approach employed to study $Na_{1.4}M_{1.6}In_{0.4}(PO_4)_3$ (M = Ti, Sn, Hf, Zr) has allowed us to establish the key structural parameters that relate the crystal structure with the Na mobility and ionic conductivity.

(2) M = Ti and Sn samples have lower ionic conductivities and higher activation energies with low Na mobility at room temperature. M = Hf and Zr samples have higher conductivities and lower activation energies with high Na mobility at room temperature.

(3) The changes in area of the T1 triangle (as simplification to define the irregular M1M2 bottleneck) correlate with variations in MAS NMR data and in the ionic conductivity properties with composition. The T1 triangle is identified as the key bottleneck in the irregular, M1M2 conduction pathway.

Acknowledgment. We thank the British Council and MEC for support from the Acciones Integradas program, HB95-1. The work in Málaga was supported by the research grant PB 93/1245 of CICYT, Ministerio de Educación y Ciencia, Spain.

CM970648J